

Promote water photosplitting via tuning quantum well states in supported metal clusters

Zijing Ding and Sheng Meng*

Beijing National Laboratory for Condensed Matter Physics, and Institute of Physics, Chinese Academy of Sciences, Beijing 100190, China

(Received 15 May 2012; published 30 July 2012)

In an effort to facilitate water photosplitting at surfaces, we identify quantum well states of magic gold clusters supported on ultrathin MgO/Ag(001) as the key to favor sunlight absorption and photocatalytic reactions. Based on density functional theory (DFT) and time-dependent DFT calculations, the adsorption geometry, electronic structures, and excited state properties of supported metal nanoparticles can be precisely controlled. By decreasing the thickness of MgO film, charge transfer to supported gold clusters, and therefore the occupation and energy spacings of quantum well states, can be gradually tuned, leading to redshifted and enhanced plasmonic excitations and optimized energy levels for water splitting.

DOI: [10.1103/PhysRevB.86.045455](https://doi.org/10.1103/PhysRevB.86.045455)

PACS number(s): 71.15.Mb

I. INTRODUCTION

Supported metal clusters on oxide surfaces are receiving intensive research interest since they can be widely used as efficient, active catalytic centers for various reactions, including CO oxidation,^{1–3} acetylene hydrochlorination,^{4–6} and the water-gas-shift reaction.⁷ Gold nanoparticles supported on titania exhibit photocatalytic activity for water splitting under uv, visible, and near-infrared light.^{8–10} When they have landed on a surface, different atomic configurations of gold cluster have been found depending on the nature of the supporting substrate, for instance, atomic chains on NiAl(110),¹¹ two-dimensional (2D) plates on alumina/NiAl(110),¹² and three-dimensional (3D) clusters on iron oxide and titania.^{13,14} In general small Au nanoparticles maintain high stability even in water solutions, making them suitable for catalytic applications.¹⁵ It has been found that excess electrons are transferred from the substrate to supported metal nanoparticles, due to electronic couplings between the substrate and the nanoparticles.^{16,17} Photocatalysis utilizing plasmonic excitation in supported metal structures has also become a hot area, thanks to dramatic field enhancements and easy tunability of metallic plasmon excitations.^{18,19} Recently it has been shown that gold nanorods on TiO₂ produce stoichiometric O₂ evolution even under near-infrared illumination via plasmon-induced excitation and charge transfer,¹⁰ Dramatic enhancement of water splitting under visible light has been discovered upon Au thin-film deposition on TiO₂, which was attributed to local field effects rather than the commonly assumed charge transfer mechanisms.⁹ Plasmon excitation of Ag nanocubes supported on alumina has been found to couple strongly with thermal energy facilitating rate-limiting O₂ dissociation at low temperatures.¹⁸ Overall the high catalytic activity of gold clusters on oxides has been attributed to structural effects (including particle size and shape)¹³ and the electronic state (charge transfer, status of metal oxidation),^{14,20} as well as to the influence of substrates. A full understanding of the mechanism of photocatalytic reactions requires a detailed knowledge about the adsorption geometry, the charge state, and the electronic structure of supported metal clusters.

Fortunately metal clusters supported by oxide thin film on metal substrate enable an *in situ* scanning tunneling microscopy (STM) investigation on their geometry, their electronic structure, and even the oxidation processes directly.

Examples include planar gold clusters with a magic number of atoms, Au₈, Au₁₄, and Au₁₈, imaged on a well-characterized MgO thin film of two monolayers (ML) supported on Ag(001),¹⁶ Quantum well states (QWS) due to the confinement effect in these artificial nanostructures have been identified. Such studies have provided atomistic information about nanoparticle/oxide interface and hint at potential ways for optimal control of reaction parameters. However, STM studies fail to provide precise identification and control of charge states of metal clusters, nor do they offer any information about optical excitation and photocatalysis mechanisms in these clusters. Indeed, the excited states of supported metal clusters, especially the influence of interface on photoabsorption and photocatalysis, are seldom investigated in either experiment or theory.

In this work we present a theoretical study on utilizing quantum well states confined in supported metal nanoparticles for promoting water photosplitting. Ways to control the geometry, the charge state, and the optical absorption of magic gold clusters supported on MgO thin film are investigated. We find that the model cluster composed by a magic number of eight Au atoms, Au₈, adopts a planar geometry on perfect MgO thin film, but retains a 3D geometry around MgO's F center (O vacancy). Electron transfer from the substrate to gold nanoparticles occurs in both cases, but differs in magnitude and spacial distribution. More importantly, we find that the amount of charge transfer, and thus the occupancy and energy spacings of QWS, can be gradually tuned by increasing the film thickness, characterized by the number of MgO layers $N = 1, 2, \dots, 10$. As a result, plasmonic excitation in supported Au₈ promotes electrons from Au *d* orbitals to discrete QWS properly positioned to drive H evolution reactions from water. With decreasing N , the major plasmonic peak is redshifted and oscillator strength is increased by 25%, matching better the terrestrial solar spectrum. Moreover, the fraction for excitation to optimal QWS for water photosplitting is greatly enhanced. These observations illustrate promising approaches in tuning excited state properties of metal clusters via engineering QWS to promote photoreactions.

II. COMPUTATIONAL METHODS

First-principles calculations have been performed within the framework of density functional theory (DFT) and

time-dependent DFT (TDDFT),^{21,22} Ground state geometries have been optimized using Projector augmented wave^{23,24} pseudopotentials and the Perdew-Burke-Ernzerhof²⁵ form for exchange-correlation functional, as implemented in the Vienna *ab initio* simulation package,²⁶ The substrate consists of one to ten monolayers of MgO thin film, in registry with three Ag(001) atomic planes with a lattice constant of 4.09 Å taken from experimental values. A (6×6) surface unit cell is constructed to hold Au₈ clusters. The plane-wave energy cutoff is 400 eV. All atoms except those in the bottom two layers of Ag are relaxed during geometry optimization until the magnitude of forces is less than 0.04 eV/Å. The optical absorption spectra are calculated within the linear response scheme based on real-time TDDFT evolution of electron wave functions using a real-space grid (spacing 0.25 Å) as basis, implemented in OCTOPUS.²⁷ The gold atom is treated using scalar-relativistic Troullier-Martins pseudopotentials, which nicely reproduce the relativistic effects of gold atoms,²⁸ Real-time propagation of electron wave functions is carried out with 25 000 steps with a time step of 0.002 fs.

III. RESULTS AND DISCUSSION

Small gold clusters exhibit unique size-dependent properties due to the presence of a large fraction of surface atoms and associated distinct electronic structures.²⁹ We first study isolated gold clusters, Au_{*n*} (*n* = 1 ~ 10), in vacuum. We find that the average cohesive energy in the Au₈ cluster is 1.96 eV per Au atom, which is higher than that in the Au₇ (1.83 eV/Au) and Au₉ (1.92 eV/Au) clusters. It agrees with previous studies, where Au₈ has been found to be more stable than Au₇ (by 0.12 eV/Au) and Au₉ (by 0.03 eV/Au).³⁰ In addition, it has also been found that small 2D structures (*n* ≤ 9) are more favorable than corresponding 3D structures in vacuum.^{30,31}

We then investigate the structure and properties of supported small gold clusters adsorbed on MgO/Ag(001). The optimized atomic configuration of the Au₈ cluster on 2 ML MgO/Ag(001) is shown in Fig. 1. On perfect MgO thin film, the Au₈ cluster retains the planar geometry, with the most stable position being the center Au atom adsorbing at the top site of the surface O atom. The adsorption energy is 0.28 eV/Au with reference to free Au₈. On the other hand, when Au₈ approaches an F-center defect (oxygen vacancy) of MgO, it adopts the 3D pyramid structure with five Au atoms close to the MgO surface and three other Au atoms staying above the surface. On the F center, the 3D structure is 0.82 eV more stable than the corresponding planar geometry, with a binding energy of 0.43 eV/Au. Furthermore, the O vacancy buried at the MgO and Ag(001) interface is stabilized by 0.72 eV compared to the O vacancy on the MgO surface (F center). And we found that the Au₈ cluster above this interface defect also adopts the planar geometry, with a binding energy of 0.34 eV/Au. These results are consistent with those reported in Refs. 2 and 16.

The planar and 3D Au₈ particles have different electronic characters when interacting with the MgO/Ag(001) substrate. Based on Bader analysis, we found there are excess electrons transferred from the substrate to Au₈, about 2.12*e* to the Au₈ 2D plate and 2.24*e* to the Au₈ 3D cluster. A similar amount of charge transfer (ca. 2.0*e*) to the Au₈ plate was found by Lin *et al.*¹⁶ This electron transfer to Au particles is supported by the

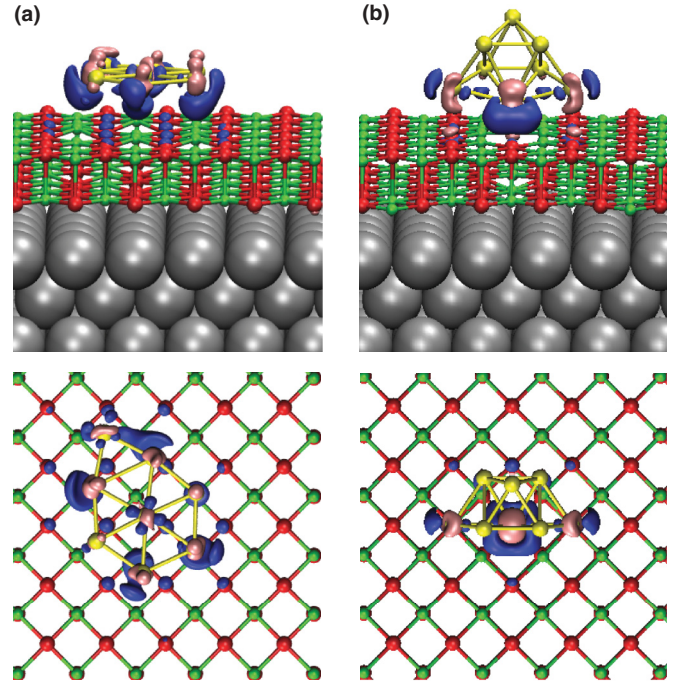


FIG. 1. (Color online) Side and top views of optimized configuration of the Au₈ magic cluster on 2 ML MgO/Ag(001) (a) with a perfect surface and (b) with an F-center defect. Green, red, yellow, and gray balls represent Mg, O, Au, and Ag atoms, respectively. The charge density difference upon adsorption is also displayed, with blue and pink clouds at isovalues of $\pm 0.025e/\text{\AA}^3$ indicating electron accumulation and depletion regions, respectively.

projected density of states plotted in Fig. 2. For both Au₈ plates on bulk MgO [3 ML MgO without Ag(001)] and on 2 ML MgO/Ag(001), the bulky Au 5*d*-orbital states (DS) are located ca. -6 eV below the vacuum level, the same as MgO valence bands. There are several QWS present within the MgO band gap, which originated from the quantum confinement effect in Au₈. They are labeled QW1, QW2, QW3, . . . , running from lower to higher energies. Compared to isolated Au₈ and Au₈ on bulk MgO without the Ag substrate, where only the first QW1 is occupied, for Au₈ on 2 ML MgO/Ag(001) both QW1 and QW2 are occupied because of $\sim 2e$ transferred to Au₈. And energy level spacings between QWS are smaller. Interestingly, the distribution of excess charges is quite different for 2D and 3D Au₈, shown by the difference charge plot in Fig. 1. The excess electrons are evenly distributed over every atom in the Au₈ plate with *s* and *d* characters; while in the Au₈ 3D cluster all charges are strongly localized on the single Au atom in the closest contact with the oxygen vacancy, due to the stronger attraction between the Au atom and the F center. The different spatial distributions of excess charges may have profound implications in catalysis and photocatalysis applications.

To illustrate whether the surface defect or the excess charge is the driving force accounting for the 2D to 3D geometry change on MgO's F center, we compare the energetics of Au₈ clusters under different conditions. The neutral Au₈ 2D plate is 0.24 eV more stable than the Au₈ 3D cluster in vacuum; the energy difference (0.50 eV) is furthered when both structures are charged with two excess electrons. Therefore excess charge

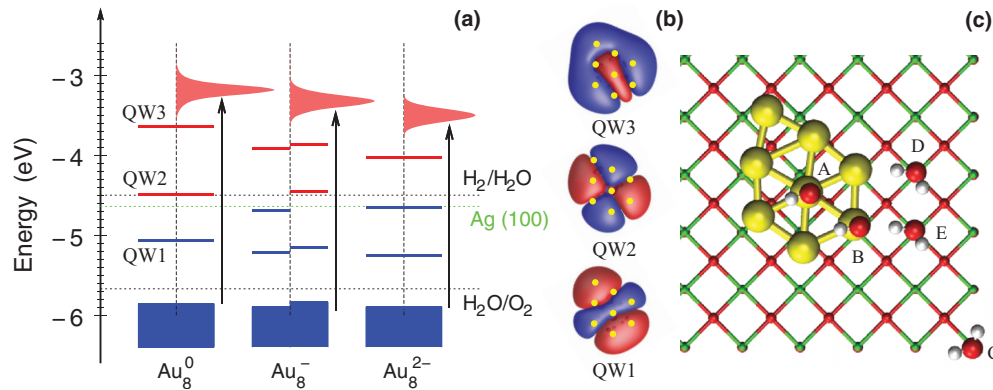


FIG. 2. (Color online) (a) Energy diagrams of supported Au_8^0 , Au_8^- , and Au_8^{2-} . The Au $5d$ orbitals comprise continuous states (blue rectangles) below discrete QWS (horizontal bars). The occupied states are shown in blue, the unoccupied states are shown as red lines, and the plasmon states shown as red peaks. All levels are relative to the vacuum level set at zero, and experimental values for H_2 and O_2 redox potential are adopted. (b) Wave functions of the first three QWS. Yellow dots indicate the position of Au atoms. (c) Different sites for water adsorption on $\text{Au}_8/2$ ML $\text{MgO}/\text{Ag}(001)$.

will favor 2D structures over 3D structures, which means charge transfer is not the reason Au_8 adopts a 3D structure. In a high-level calculation, Au_8^- is also found to be planar.³¹ The atomic structure of the F-center defect is the main cause of the Au_8 plate changing into a 3D isomer. This fact manifests the importance of surface atomic structure for maintaining the geometry, the shape, and, in turn, the electronic properties of metal clusters. We note that the larger clusters, Au_{14} and Au_{18} , are 3D in vacuum³¹ but all are planar on 2 ML $\text{MgO}/\text{Ag}(001)$,¹⁶ as a result of surface interaction and charge transfer. Since planar Au_8 , whose structure has been experimentally confirmed, is dominant on perfect surfaces, we mainly concentrate on the Au_8 plate as our model for supported metal clusters.

We explore the possibility of employing supported Au magic clusters for water photosplitting. Decomposing water on oxide films has been a research focus currently under intensive investigation. It has been shown that MgO thin film can significantly decrease water dissociation barriers using thermal energies as input.^{20,32} However, the large band gap of oxides (>6 eV) prevents any effective photo reactivity under solar irradiation. To solve the problem the presence of metal nanoparticles on oxides could be critical in several aspects:

(i) dramatic enhancement in visible light absorption due to high optical sensitivity of metal nanoparticles, other than the wide gap oxides, to sunlight;

(ii) prolonged lifetime upon electron excitation into discrete QWS, thanks to quantum confinement in nanoparticles, different from rapid damping in bulk metals;

(iii) tunable chemical reactivity of nanoparticles in ground and excited states by manipulating charge transfer and photoexcitation via controlling the size, shape, and electronic properties of nanoparticles.

We expect QWS present in Au_8 are well suited to promote water photosplitting on MgO thin films.

We first calculate the interaction between water molecules and the Au_8 plate supported on MgO thin film. Numerous sites potential for water adsorption are explored. We found that direct water adsorption on the top of the Au_8 cluster is not favored, with binding energies E_{ads} being as small as 86 meV [above center Au atom, site A in Fig. 2(c)] and

137 meV (on the Au atom at the edge of the cluster, site B). This is consistent with weak interactions between water and $\text{Au}(111)$ ($E_{\text{ads}} \sim 0.11$ eV).³³ On the other hand, water adsorption is dramatically enhanced around MgO -supported Au nanoparticles: E_{ads} increases from 360 meV on perfect MgO (site C) to 620 meV (site D) and 780 meV (site E) for water on the periphery of Au_8 , where water sits on the top of surface Mg atoms closest to Au_8 . Water couples strongly to the QWS of Au_8 : on site E, there are more electrons pointing to the H of H_2O in QW1 and QW2 states than on site D, where there is a dip in wave function distribution around the same H. This leads to more excess electrons on the Au atom nearest to site E ($0.41e$) than on that nearest to site D ($0.21e$), resulting in a higher water binding energy on site E. The interaction between H_2O and QWS orients the OH bond in water, pointing to negatively charged Au atoms, elongating the OH bond length from 0.97 to 1.02 Å, and shortening the H-Au bond length to 2.27 Å (see Table I). This interaction would favor water splitting. Our calculation of H^+ adsorption on the Au_8 plate shows the equilibrium distance between the H^+ and Au atoms is 1.63 Å. Only about 0.64 Å is needed for H to move into a dissociated state. The nudged elastic band calculations³⁴ show that the energy barrier for water dissociation is quite small, ~ 0.80 eV. Therefore the preferential H_2O attachment to the electron-rich boundary of supported gold clusters, similar to the case of CO adsorption,³⁵ would facilitate water splitting.

TABLE I. Adsorption energy (E_{ads}) and geometry parameters for water molecule adsorption on different sites of 2 ML $\text{MgO}/\text{Ag}(001)$. The subscripts O_w , H_a , and H_b stand for the O atom and the two H atoms in water, respectively. Distances are in angstroms and angles are in degrees. The adsorption sites are shown in Fig. 2(c).

| Sites | E_{ads} (meV) | $d_{O_w-H_a}$ | $d_{O_w-H_b}$ | $\angle H_a O_w H_b$ | d_{O_w-Mg} | d_{H_a-Au} |
|-------|------------------------|---------------|---------------|----------------------|--------------|--------------|
| A | 86 | 0.98 | 0.97 | 103.4 | | 2.55 |
| B | 137 | 0.98 | 0.98 | 103.6 | | 2.53 |
| C | 360 | 0.97 | 0.97 | 106.1 | 2.21 | |
| D | 620 | 1.01 | 0.98 | 103.8 | 2.13 | 2.21 |
| E | 780 | 1.02 | 0.97 | 105.5 | 2.12 | 2.23 |

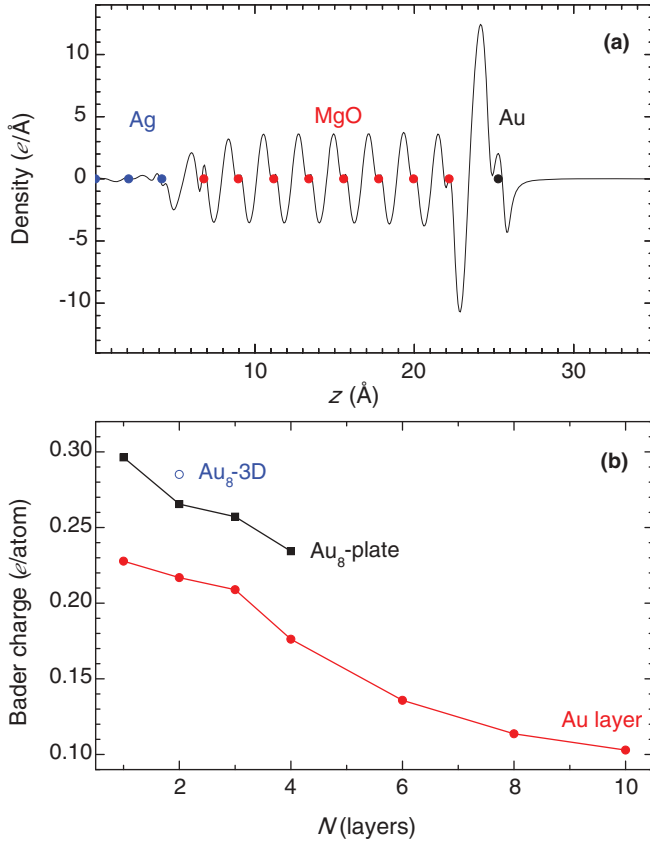


FIG. 3. (Color online) (a) Plane-averaged electron density difference along the surface normal $\Delta\rho = \rho[\text{Au}/\text{substrate}] - \rho[\text{substrate}] - \rho[\text{Au}]$, showing charge displacement upon Au monolayer adsorption on 8 ML MgO/Ag(001). (b) Calculated excess electrons as a function of the number of MgO layers, N , for the Au monolayer (solid circles), the Au₈ plate (squares), and the 3D cluster (empty circles) on MgO/Ag(001).

We search for ways to control electronic interaction and interface charge transfer for surface QWS. We then look at the influence of MgO film thickness on charge transfer between the substrate and the QWS in gold clusters. To make the systemic investigation affordable, we also build a simplified (2×2) surface unit cell to model Au monolayers on MgO/Ag, with MgO thickness ranging from 1 to 10 ML. Figure 3(a) shows the one-dimensional, plane-averaged electron density difference upon Au adsorption on 8 ML MgO/Ag(001). A strong charge polarization is found, where MgO serves as a dielectric buffer and Au as an electron acceptor with the majority electron density located above the substrate and close to Au. A net electron transfer of $\sim 0.11e$ per Au atom from the substrate is found in this case.

The amount of charge transfer as a function of the number of MgO layers, N , is further displayed in Fig. 3(b). With N increasing, charge accumulation on Au drops from $\sim 0.23e$ per Au ($N = 1$) to $0.10e$ per Au ($N = 10$), following a trend close to exponential decay. We also calculate charge transfer to a finite Au₈ plate as a function of N for thinner MgO layers. A similar trend is found, though the amount of charge transfer is enhanced by $\sim 30\%$. The charge transfer enhancement comes from quantum confinement in Au₈ as compared to Au layers. Excess electrons transferred to the Au₈ plate range from $0.30e$

($N = 1$) to $0.23e$ ($N = 4$) per Au atom. The same trend is also found for Au₈ on a different substrate, MgO/Mo.¹⁷ From these trends, we estimate for 8 ML MgO, there is about $\sim 1e$ ($0.13e$ per Au atom) transferred to Au₈. The 3D cluster on the F center accepts more electrons than the 2D plate, but mostly localized on the single Au atom in contact with the defect [Fig. 1(b), lower panel]. Consequently, we find a way to control interface charge transfer: charge accumulation on supported Au clusters can be tuned by adjusting the thickness of MgO layers.

Understanding excited state properties of QWS in gold magic clusters is necessary for water photosplitting. We calculate the optical absorption spectrum of the Au₈ plate using real-time TDDFT. The effects of interface interaction, especially tunable charge transfer to supported Au₈ are considered. Since the net charge from the substrate is evenly distributed, an isolated nanoparticle with extra charges represents a reasonable model. Moreover, the optical response of MgO thin film below 7.0 eV is negligible (MgO band gap, ~ 7.8 eV), and the Ag substrate imposes a minor influence below its surface plasmon energy of 3.8 eV (Ref. 36) except for providing excess electrons. We therefore neglect the structure of the substrate, while taking charge transfer and adsorption geometry into consideration to make TDDFT calculations affordable. Due to strong localization of excess charges, this simplification does not apply to the case of Au₈ 3D clusters on F centers.

Figure 4 displays the calculated absorption spectrum of the Au₈ plate with zero, one, and two excess electrons, corresponding to adsorption on the MgO film with a thickness of infinity, ~ 8 ML, and ~ 2 ML, respectively. The absorption spectra

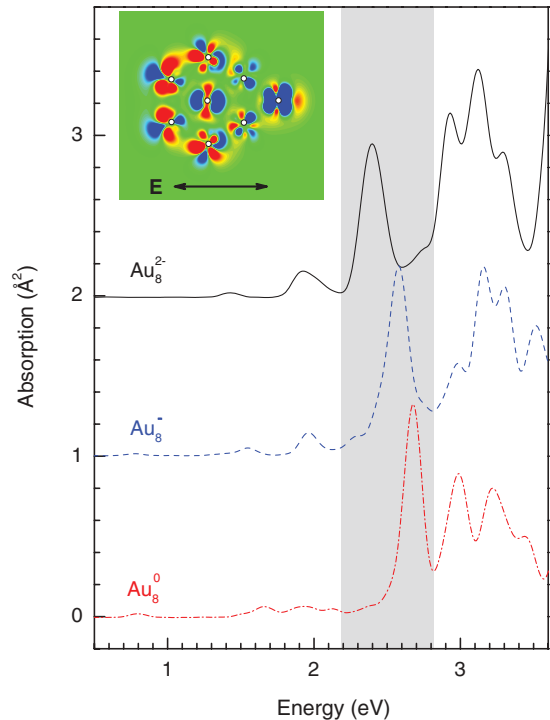


FIG. 4. (Color online) Optical absorption of supported Au₈ plate in different charge states. The inset shows the induced charge density for Au₈ excited at a plasmon energy of $\omega_p = 2.68$ eV. The empty circles denote the positions of Au atoms.

TABLE II. Parameters for the major plasmon excitation under visible light in the Au₈ plate with different charge states. ω_p is the plasmon energy; $\Delta\omega$ is the full-width at half maximum of the peak. The excitation comprises contributions from 5*d*-orbital states (DS) to the second quantum well state (QW2), from DS to the third quantum well state (QW3), from DS to the fourth quantum well state (QW4), and from the first quantum well state (QW1) to QW4. Fractions of different contributions are listed.

| | Au ₈ ⁰ | Au ₈ ⁻ | Au ₈ ²⁻ |
|---------------------|------------------------------|------------------------------|-------------------------------|
| ω_p (eV) | 2.68 | 2.58 | 2.40 |
| $\Delta\omega$ (eV) | 0.16 | 0.18 | 0.20 |
| Oscillator strength | 0.40 | 0.42 | 0.50 |
| DS → QW2 | 30.8% | 16.6% | |
| DS → QW3 | 25.1% | 47.1% | 60.8% |
| DS → QW4 | 6.44% | 16.3% | 38.2% |
| QW1 → QW4 | 37.5% | 19.5% | 0.61% |

can be divided into two regimes with distinct features: the single-particle excitation regime (<2.2 eV) and the plasmonic excitation regime (>2.2 eV). The low-energy single-particle excitations come from transitions between discrete QWS of the Au₈ cluster. For instance, transition from the highest occupied molecular orbital (HOMO) to the lowest unoccupied molecular orbital (LUMO) occurs at 0.8 eV. Comparing this value to the HOMO-LUMO energy gap calculated in ground state DFT, which is 0.56 eV, we estimate that the error for the energy levels calculated in ground state DFT, as presented in Fig. 2(a), is on the order of 0.2–0.3 eV. This peak diminishes in Au₈⁻ and completely disappears in Au₈²⁻ when the LUMO is fully occupied.

Excitations at higher energy come from collective electronic excitations in the Au₈ cluster, namely, plasmon excitations. A major peak is found at 2.68 eV for Au₈⁰, 2.58 eV for Au₈⁻, and 2.40 eV for Au₈²⁻. Together with some additional peaks around 3 eV, plasmon modes of Au₈ clusters dominate visible light absorption within the energy range of 1.6–3.1 eV. Interestingly the redshift of the major peak with increased electron density is contrary to predictions in classical theory, which manifest the necessity of quantum treatment of plasmon excitation in small finite clusters. A peak broadening is also found, with full-width at half maximum $\Delta\omega$ being 0.16 eV for Au₈⁰, 0.18 eV for Au₈⁻, and 0.20 eV for Au₈²⁻. As a result, the oscillator strength for visible light absorption increases with extra charges, 0.40 for Au₈⁰, 0.42 for Au₈⁻, and 0.50 for Au₈²⁻. To illustrate its nature, the induced density oscillation for this plasmon mode is shown in the inset of Fig. 4, which displays the polarization of 5*d* orbitals for all Au atoms. The redshift of the plasmon peak results from decreased gaps between the QWS and DS with increasing extra charges [Fig. 2(a)]. The optical absorption of gold nanoparticles is thus tuned by the interface charge transfer, toward a better match and larger overlap with the solar spectrum, whose maximum intensity is located at 2.48 eV.

The involvement of Au 5*d* orbitals is further confirmed by decomposing excited states into transitions between Kohn-Sham orbitals. Table II summarizes major contributions in the energy range ($\omega_p + \Delta\omega$, $\omega_p - \Delta\omega$) for the plasmon excitation

at $\omega_p = 2.4\text{--}2.7$ eV. Detailed analysis shows that this mode in neutral Au₈⁰ comprises four major contributions:

- (1) collective excitations from 5*d*-orbital states DS to QW2 (fraction of contribution, 30.8%),
- (2) collective excitations from DS to QW3 (fraction, 25.1%),
- (3) collective excitations from DS to QW4 (fraction, 6.44%),
- (4) a single excitation from QW1 to QW4 (fraction, 37.5%).

As the Au₈ cluster receives one and two more electrons, the contribution of DS → QW2 diminishes due to the occupation of QW2. In contrast, the contribution from DS → QW3 collective excitations becomes dominant, increasing from 25.1% to 60.8%. The contribution from excitations to QW4 retains at a fraction of ~40% for all cases, however, it also gradually shifts from a single-particle QW1 → QW4 excitation to a more collective DS → QW4 character. It is well known that collective plasmon excitations rapidly damp into electron-hole pairs; we expect that for Au₈²⁻ the probability of excited plasmon damping into a hot electron in QW3 and a hole in DS is high (60%). This hot electron in QW3 would facilitate water splitting since its energy is much higher than the standard hydrogen potential for H₂/H₂O evolution at -4.5 eV (see Fig. 2). Here the energy levels are aligned relative to the vacuum level set to be zero, and the experimental value for H₂/H₂O redox is adopted. For comparison QW2 would be too low in energy without any overpotential to the H₂/H₂O redox level.

Enhanced visible light absorption and excitation to high-lying QWS by extra charges of supported gold cluster have a profound implication for photocatalysis including water splitting.^{8,9} Au₈ clusters exhibit excitations between discrete QWS, as well as plasmon excitations mainly involving DS → QWS modes. Plasmon excitations promote DS electrons to high-energy states (red peaks in Fig. 2), which rapidly (~30 fs, estimated from the intrinsic width of plasmon peaks) damp into electron-hole pairs and generate hot electrons supplying the extra energy needed for H₂ reduction. The plasmon energy, well above the H₂/H₂O redox potential, is high enough to overcome the barrier for water splitting (~0.8 eV). Moreover, by tuning the amount of charge transfer, the excited state level can be tuned to be closer to the H₂ redox level while maintaining a better match to the solar spectrum, favoring optimal solar-hydrogen conversion. The 5*d*-orbital DS states comprise continuous states lying below QWS and but close to the MgO valence bands, which are lower than the O₂ electrode potential, i.e., the H₂O/O₂ redox potential at -5.73 eV. Thus water oxidation might occur via the Au nanoparticle itself, as shown experimentally,¹⁰ or via hole transfer to MgO surfaces. With the above preliminary analysis on water adsorption and decomposition, our research hints at useful application and further optimization for water photosplitting based on supported gold clusters.

IV. CONCLUSION

In conclusion, we have applied quantum mechanical simulations based on DFT and TDDFT to investigate electronic structure and excitation of Au₈ supported on MgO thin film. We found the presence of QWS can be utilized to promote water photosplitting thanks to enhanced water binding, visible

light absorption, and optimized energy levels. It was shown that MgO substrate can change the shape, charge states, and optical properties of supported gold clusters, by reducing the number of MgO layers. In this way, the major plasmonic peak has a redshift from 2.68 to 2.40 eV and a 25% increase in oscillator strength, as well as an increased fraction excited to energy levels optimal for water splitting, matching better the solar spectrum. As observed from our study, the excited state properties of gold clusters can be controlled by surface interaction and the thickness of MgO film. This practice of

tuning QWS for water photosplitting is generally applicable to many other systems and photoreactions.

ACKNOWLEDGMENTS

The authors are indebted S. W. Gao, Y. Gao, P. Song, and Y. Jiao for valuable discussions. We acknowledge financial support from the NSFC (Grant No. 11074287), MOST (Grant No. 2012CB921403), and the Hundred Talents Program and Knowledge Innovation Project of the CAS.

*Corresponding author: smeng@iphy.ac.cn

- ¹M. Haruta, T. Kobayashi, H. Sano, and N. Yamada, *Chem. Lett.* **16**, 405 (1987).
- ²B. Yoon, H. Hakkinen, U. Landman, A. S. Worz, J.-M. Antonietti, S. Abbet, K. Judai, and U. Heiz, *Science* **307**, 403 (2005).
- ³M. Arenz, U. Landman, and U. Heiz, *Chem. Phys. Chem.* **9**, 1871 (2006).
- ⁴G. J. Hutchings and M. Haruta, *Appl. Catal., A* **291**, 2 (2005).
- ⁵G. J. Hutchings, *J. Catal.* **96**, 292 (1985).
- ⁶B. Nkosi, N. J. Coville, G. J. Hutchings, M. D. Adams, J. Friedl, and F. Wagner, *J. Catal.* **128**, 292 (1991).
- ⁷F. Boccuzza, A. Chiorino, M. Manzolia, D. Andreevab, and T. Tabakovab, *J. Catal.* **188**, 176 (1999).
- ⁸S. V. Awate, S. S. Deshpande, K. Rakesh, P. Dhanasekaran, and N. M. Gupta, *Phys. Chem. Chem. Phys.* **13**, 11329 (2011).
- ⁹Z. Liu, W. Hou, P. Pavaskar, M. Aykol, and S. B. Cronin, *Nano Lett.* **11**, 1111 (2011).
- ¹⁰Y. Nishijima, K. Ueno, Y. Kotake, K. Murakoshi, H. Inoue, and H. Misawa, *J. Phys. Chem. Lett.* **3**, 1248 (2012).
- ¹¹T. M. Wallis, N. Nilius, and W. Ho, *Phys. Rev. Lett.* **89**, 236802 (2002).
- ¹²N. Nilius, M. V. Ganduglia-Pirovano, V. Brazdova, M. Kulawik, J. Sauer, and H.-J. Freund, *Phys. Rev. Lett.* **100**, 096802 (2008).
- ¹³M. S. Chen and D. W. Goodman, *Science* **306**, 252 (2004).
- ¹⁴A. A. Herzog, C. J. Kiely, A. F. Carley, P. Landon, and G. J. Hutchings, *Science* **321**, 1331 (2008).
- ¹⁵J. Zheng, C. Zhang, and R. M. Dickson, *Phys. Rev. Lett.* **93**, 077402 (2004).
- ¹⁶X. Lin, N. Nilius, H. J. Freund, M. Walter, P. Frondelius, K. Honkala, and H. Hakkinen, *Phys. Rev. Lett.* **102**, 206801 (2009).
- ¹⁷D. Ricci, A. Bongiorno, G. Pacchioni, and U. Landman, *Phys. Rev. Lett.* **97**, 036106 (2006).
- ¹⁸S. Linic, P. Christopher, and D. B. Ingram, *Nat. Mater.* **10**, 911 (2011).
- ¹⁹T. Olsen and J. Schiøtz, *Phys. Rev. Lett.* **103**, 238301 (2009).
- ²⁰H.-J. Shin, J. Jung, K. Motobayashi, S. Yanagisawa, Y. Morikawa, Y. Kim, and M. Kawai, *Nat. Mater.* **9**, 442 (2010).
- ²¹W. Kohn and L. J. Sham, *Phys. Rev.* **140**, A1133 (1965).
- ²²M. A. L. Marques and E. K. U. Gross, *Annu. Rev. Phys. Chem.* **55**, 427 (2004).
- ²³D. Vanderbilt, *Phys. Rev. B* **41**, 7892 (1990).
- ²⁴P. E. Blöchl, *Phys. Rev. B* **50**, 17953 (1994).
- ²⁵J. P. Perdew, K. Burke, and M. Ernzerhof, *Phys. Rev. Lett.* **77**, 3865 (1996).
- ²⁶G. Kresse and J. Hafner, *Phys. Rev. B* **47**, 558 (1993).
- ²⁷M. A. L. Marques, A. Castro, G. F. Bertsch, and A. Rubio, *Comput. Phys. Commun.* **151**, 60 (2003).
- ²⁸N. Troullier and J. L. Martins, *Phys. Rev. B* **43**, 1993 (1991).
- ²⁹*Metal Clusters*, edited by W. Ekaradt (Wiley, Chichester, 1999).
- ³⁰J. C. Idrobo, W. Walkosz, S. F. Yip, S. Ögüt, J. Wang, and J. Jellinek, *Phys. Rev. B* **76**, 205422 (2007).
- ³¹L. Ferrighi, B. Hammer, and G. K. H. Madsen, *J. Am. Chem. Soc.* **131**, 10605 (2005).
- ³²J. Jung, H.-J. Shin, Y. Kim, and M. Kawai, *Phys. Rev. B* **82**, 085413 (2010).
- ³³S. Meng, E. G. Wang, and S. Gao, *Phys. Rev. B* **69**, 195404 (2004).
- ³⁴G. Henkelman, B. P. Uberuaga, and H. Jónsson, *J. Chem. Phys.* **113**, 9901 (2000).
- ³⁵X. Lin, B. Yang, H.-M. Benia *et al.*, *J. Am. Chem. Soc.* **132**, 7745 (2010).
- ³⁶H. Ehrenreich and H. R. Philipp, *Phys. Rev.* **128**, 1622 (1962).